FUNCTIONAL OPTICAL IMAGING OF INTRINSIC SIGNALS IN CEREBRAL CORTEX

L. E. HALLUM
S. C. CHEN
S. L. CLOHERTY
University of New South Wales
Sydney, Australia
and
University of Newcastle
Callaghan, Australia
J. W. MORLEY
University of New South Wales
Sydney, Australia
G. J. SUANING
University of Newcastle
Callaghan, Australia
and
University of New South Wales
Sydney, Australia
N. H. LOVELL
University of New South Wales
Sydney, Australia
and
National ICT Australia
Eveleigh, Australia

1. BACKGROUND

In the early nineteenth century, Franz Gall, a German-born physician and neuroanatomist who studied and worked in Vienna, proposed that specific functions or behaviors are controlled by particular regions of the cerebral cortex. Although Gall extended this proposition to develop the (incorrect) doctrine of phrenology, it was the first account of localization of function in the cerebral cortex. Forty years later Gall's ideas were extended by Paul Pierre Broca, who in 1861 published an account of a patient who could understand language but could not speak. Postmortem examination of the patient's brain showed a lesion in the posterior area of the frontal lobes, an area that has become known as Broca's area. This intriguing finding led to the search for more functionally distinct regions of the cerebral cortex and, in 1870, Fritsch and Hitzig reported that electrically stimulating the precentral gyrus in the dog resulted in movements of the contralateral limb. Fritsch and Hitzig had found what is now known as the primary motor cortex. Investigation of localized functional regions of the cerebral cortex increased at a rapid pace and by the mid-twentieth century it was well established that the cerebral cortex could be divided into discrete regions on the basis of cytoarchitectonics (type, density, and layering of cells) and physiological function. Localization of function in the cerebral cortex is perhaps best demonstrated in the mammalian visual cortex, where in the primate and presumably the human, more than 30 distinct cortical regions associated with the analysis of visual information exist.

The localization of function in the cerebral cortex has traditionally relied on techniques such as lesion studies, neuroanatomical tract tracing and single-cell electrophysiology in animal-based experiments, or on clinical studies where behavioral symptoms are correlated with postmortem findings of underlying cortical pathology or where specific regions of the cerebral cortex are electrically stimulated during neurosurgical procedures for disorders such as epilepsy. In addition to these techniques, a number of imaging techniques are now available, including positron emission tomography (PET), functional magnetic resonance imaging (fMRI), and optical imaging of intrinsic signals (OIIS). In functional imaging of the cerebral cortex, the relationship between regional cerebral blood flow (rCBF) and function is exploited to correlate localized cortical activity with physiological function.

OIIS is a minimally invasive means of determining patterns of neural activity over large areas of the cortex (typically on the order of 25 mm^2) with resolution as fine as tens of micrometers. The signal is manifest as a darkening of the cortex; that is, it occurs when the light absorption of the tissue increases and its reflectance decreases. These light-related phenomena closely correlate with underlying neural activity and are largely because of the fact that cerebral blood flow (CBF) and energy metabolism are regulated at such a fine scale.

2. THEORY

In order to illustrate the components of the intrinsic signal and its underlying mechanisms, it is convenient to consider an example. Figure 1 shows ocular dominance columns in the visual cortex of the cat. In response to a brief visual stimulation of one eye, a column of some thousands of cortical neurons becomes active. This activity requires energy; an integral part of cerebral energy metabolism is a reaction involving oxygen and glucose. Specifically, more than 85% of cerebral glucose is used by neurons, largely for the maintenance of (presynaptic) membrane voltages and the restoration of ion gradients affected by synaptic activity (1). The column, therefore, draws oxygen from the local capillary bed, where hemoglobin (the protein in red blood cells that binds to oxygen) becomes deoxygenated leading to an increase in the concentration of deoxyhemoglobin.

Several hundred milliseconds subsequent to synaptic activity onset, rCBF and blood volume increase (hyperemia). Although the exact mechanism driving the increase is unknown (some argue that the trigger is increased tension of carbon dioxide, a byproduct of cerebral metabolism, or reduced oxygen tension in the microvasculature, whereas others argue neurogenic triggers), this transient hyperemia meets, and indeed exceeds, local oxygen demand. Therefore, ultimately and somewhat paradoxically, after an initial increase, the response to increased synaptic activity is a decreased concentration of deoxyhemoglobin and an increased concentration of oxyhemoglobin. This hyperemic transient then decays over the course of 10 to 30 s.

The sequence of events—synaptic activity, hypo-oxygenation, and delayed hyperemia—affects the tissue's absorption and reflection of light, which is first because neuropil (areas of cerebral gray matter rich in synapses,

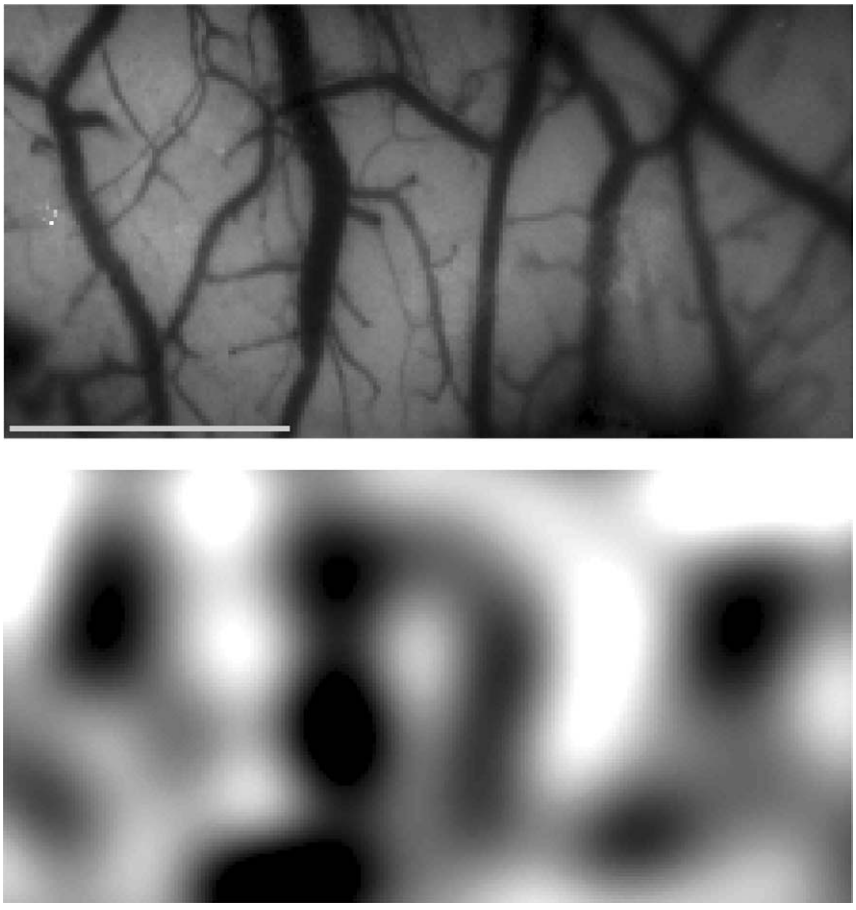

Figure 1. Ocular dominance columns in the primary visual cortex of the cat (unpublished data, present authors). The top panel shows a "plain view" of the cortex (illumination at approx. 540 nm). In the lower panel, those areas depicted light are areas of cortex that respond preferentially to visual stimulation of the right eye, forming so-called columns (which extend several millimeters normally to the surface of the cortex). Areas depicted dark respond preferentially to visual stimulation of the left eye. The stimuli used were square-wave gratings with period 0.2 cycles per degree, duty cycle 0.5, and drift rate 2 cycles per second. Illumination was at a wavelength of

dendrites, and axons) scatters light when activated. This phenomenon is believed to be associated with neurotransmitter release and with ion and water movement and related shrinkage of the extracellular space (2,3).

Second, the level of oxygenation of hemoglobin in the local capillary bed, assuming the total concentration of hemoglobin remains constant, affects the absorption of light. Figure 2 (4) shows the absorption spectra of oxyhemoglobin and deoxyhemoglobin. If the cortex was illuminated at 605 nm, for example, the increased deoxyhemoglobin concentration associated with the initial hypo-oxygenation and the concomitant decreased oxyhemoglobin concentration make for increased light absorptivity; at 605 nm, deoxyhemoglobin is approximately five-fold more absorptive than oxyhemoglobin. For this reason, if the cortex is illuminated at an isobestic wavelength such as 570 nm (where the absorptivities of oxyhemoglobin and deoxyhemoglobin are equal; see Fig. 2), the initial deoxygenation cannot be measured.

Third, note that the ordinate units in Fig. 2 are *L / mmol / cm*. Therefore, increased blood volume makes for increased absorption. Of the three compartments comprising the cerebral microvasculature, the arteriolar, capillary, and venular, the volume increase is believed to take place for the most part in arterioles and capillaries (5,6). For the former, this is due to dilation and for the latter, to recruitment (6,7). In highly vascular areas, the measured change in reflectance may be dominated by the blood

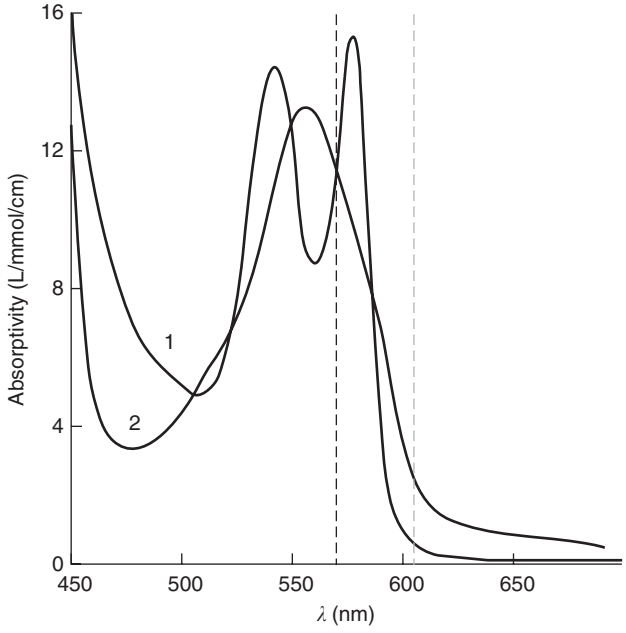

Figure 2. Absorption spectra for oxy- (1) and deoxyhemoglobin (2). The left-most vertical, dashed line indicates an isobestic wavelength of 570 nm (i.e., where the absorptivity of oxy- and deoxyhemoglobin are equal). The right-most vertical, dashed line indicates a commonly used imaging wavelength of 605 nm (spectral data taken from Ref. 4).

volume component and only weakly correlated with localized neural activity. Therefore, special care must be taken in the image processing phase to isolate the signal of interest (see the discussion on single condition maps in the section on Image Processing below).

Although the precise composition of the intrinsic signal and the relative contribution of its components are subject to ongoing study, the following physical model, or slight variations of it, is well held (8):

$$\Delta R(\lambda, t) \approx K_o(t)\varepsilon_o(\lambda) + K_d(t)\varepsilon_d(\lambda) + LS(t),$$

where ΔR is the intrinsic signal, a function of wavelength, and time relative to the stimulus onset; K_o is the oxyhemoglobin concentration, an approximately linear function of time relative to stimulus onset; ε_o is the absorptivity of oxyhemoglobin, a function of applied wavelength; K_d and ε_d are the equivalent concentration and absorptivity for deoxyhemoglobin; and LS is the light scattering component, a wavelength-independent function of time since stimulus onset. The light-scattering component of the intrinsic signal is the most spatially correlated with synaptic activity. As the amplitude of this component is invariant with respect to wavelength, it dominates the intrinsic signal at near red and infrared wavelengths, where the absorptivity of oxy- and deoxyhemoglobin and their contributions to the intrinsic signal are comparatively small. Mayhew et al. (9) estimated the light-scattering component to be 50 times that of the oxyhemoglobin and deoxyhemoglobin components at 590 nm in anesthetized rat somatosensory cortex. At shorter wavelengths, the deoxyhemoglobin and oxyhemoglobin components make a greater contribution to the signal, which is readily reconciled with the amplitude of the spectra shown in Fig. 2, where at shorter wavelengths, deoxyhemoglobin and oxyhemoglobin are significantly more absorptive. Of the two "blood" components, the deoxyhemoglobin component is the most tightly spatially correlated with synaptic activity, whereas the oxyhemoglobin component is somewhat coarse (10). Whereas the deoxyhemoglobin signal is driven by the early hypo-oxygenation, the oxyhemoglobin component is driven by the delayed hyperemia. To borrow the analogy of Malonek and Grinvald (11), the hyperemic oxygenation of the cortex is coarse, a case of the entire garden being watered for the sake of a single thirsty flower. Malonek and Grinvald (11) reported the oxyhemoglobin component, in the cat visual cortex, as being approximately an order of magnitude greater than the deoxyhemoglobin component.

3. TECHNIQUE AND EQUIPMENT

The aim of this section is not an exhaustive review of the method (for an exhaustive review, the reader is referred to Grinvald et al. (12) among others). Rather, the aim is to canvas the typical optical imaging setup, which poses an involved biomedical engineering problem drawing from a broad set of skills, including animal physiology, optics, electrical engineering, and image processing. A schematic of the optical imaging setup is shown in Fig. 3. In short, a brief sensory stimulus is presented to the animal while the cortex is imaged. The cortex is exposed via a small trephine hole and illuminated at a single wavelength. The acquired data, comprising prestimulus, or resting-state images, plus images of the neural response to the sensory stimulus, are then analyzed with reference to the stimulus onset.

The requisite synchronization of the stimulus and recording devices is not uncommon to neurophysiological techniques generally, such as single-cell electrode recordings, scalp recordings of evoked potentials, fMRI, or PET imaging. Likewise, the stimuli typically employed (e.g., the mechanical stimulation of a single rat whisker, or visual stimulation of the cat retina) are well-established in the neurophysiological literature. Specific to optical imaging, however, is the amount of data involved and the numerous sources of noise. The significant noise sources include: (1) thermal noise intrinsic to the imaging device and to the light source; (2) quantum noise associated with low light levels; (3) microscopic movement of the tissue in question (inevitable where *in vivo* preparations are concerned); and (4) biological variability of the animal (e.g., variability in microvasculature perfusion that is uncorrelated with synaptic activity). These noise sources are typically difficult to mitigate beyond the order of magnitude of the small signal of interest. Some direct measures involve the preparation of the animal; a bilateral pneumothorax is commonly undertaken to limit the translation of intrapleural pressure to the cerebrospinal space, which in turn reduces brain pulsation. To further reduce artifacts caused by brain pulsation, stimulus and acquisition are often synchronized to the cardiac and respiratory cycles of the animal. Further, multiple imaging sequences for a given stimulus condition are often required to facilitate averaging. As a result, the amount of data the experimenter acquires is often significant. For example, examining a single cortical response to a single stimulus condition may involve in excess of two gigabytes of data acquired over a period of tens of minutes. Given the state of technology at the time of writing, this fact poses considerable demands on the computer operating the imaging device. Other means typically employed to reduce artifacts and noise are discussed below with reference to specific elements of the experimental setup. Additionally, a novel data acquisition technique was recently proposed by Kalatsky and Stryker (13), who employed continuous data acquisition with periodic presentation of the stimulus condition to mitigate the effects of cardiac and respiratory artifacts. By controlling the period of the stimulus presentation, they were able to localize the spectral content of the response in an area of the spectrum free of noise and artifacts.

3.1. Cranial Window

At its simplest, the cranial window involves a thin layer of mineral oil applied to the tissue, which is then covered with a microscope cover slip (14) (in this case the dura mater is left intact). More typically, a length of stainless-steel tube (height <1 cm; inside diameter ~ 2.5 cm) is secured to the skull by way of bone or dental cement, the

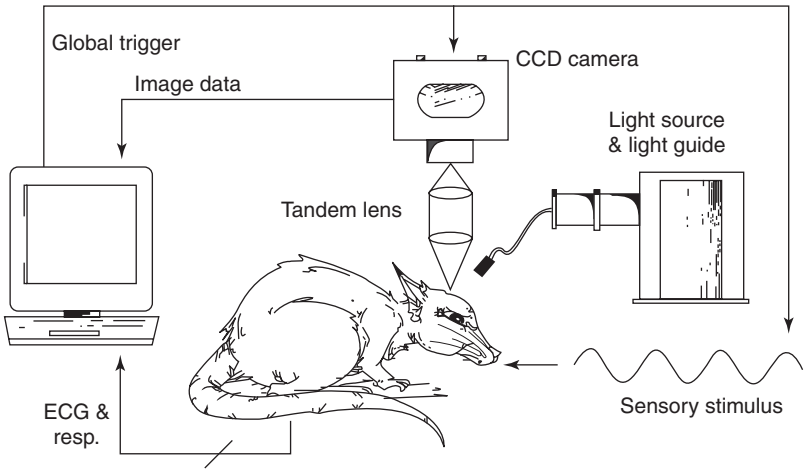

Figure 3. Schematic of a typical optical imaging setup. The sensory stimulus and subsequent image acquisition may be gated against electrocardiogram (ECG) and respiration in order to reduce motion artifact.

skull being exposed after the scalp is reflected. Trephination and reflection of the dura is then performed within the tube and the tube is then filled with mineral oil and capped with a microscope slide. Aside from guarding against tissue dehydration, the column of fluid provides some hydrostatic pressure, which mitigates noise caused by brain pulsation. The chamber may involve ports for cycling of mineral oil and removal of air bubbles. Some chronic preparations involve the placement of an artificial dura, made from thin, transparent silicone rubber, prior to filling the chamber (8), which, with the addition of the local administration of antibiotics, guards against infection. Cranial windows are reviewed in Kontos (15).

3.2. Illumination

The exposed cortex is illuminated from above, so-called epi-illumination. The light source is typically incandescent and broad-spectrum (e.g., a 100-watt tungsten-halogen lamp). That is, power is distributed approximately equally across visible and infrared wavelengths. Stable epi-illumination is of paramount importance; therefore, the power supply to the light source is typically regulated such that fluctuations are limited to less than one part in 1000. Alternatively, the light source may be supplied by a deep-cycle battery. A flexible light guide and an interference filter are used in combination with the light source so as to target specific components of the intrinsic signal. For example, an orange-red filter with peak at 605 nm and width-at-half-height equal to 10 nm may be used to investigate the initial hypo-oxygenation, as mentioned in the Theory section. Note that the cortex may be illuminated by broad-spectrum light and filtering applied by way of attachments to the camera (or imaging device) itself. The angle of incident light and its intensity are important factors in retrieving the intrinsic signal. Alternative means of illumination, such as light-emitting diodes (LEDs), have also been employed successfully by some investigators, including the present authors.

3.3. Camera Lens

A lensing system is required to focus the cortex onto the imaging device. A "tandem lens" is commonly used (16), wherein an adaptor connects two lenses front-to-front, an objective lens (closest to the tissue) and an imaging lens (attached to the imaging device). The tandem lens allows shallow depth of field (DoF) and magnification (M) according to the focal lengths of the lenses:

$$M = \frac{f_{imaging}}{f_{objective}}.$$

It is common practice that two identical, commercially available, 50 mm lenses are employed to form the tandem lens, with the resulting magnification being 1. The macroscope allows minimal DoF because of the high f-stop numbers it obtains; f-stop is the ratio of focal length to aperture diameter. DoF may be approximated as follows (17, p. 187):

$$DoF \approx 2\frac{CoC}{M^2}(F_{imaging} + MF_{objective}),$$

where $F_{imaging}$ and $F_{objective}$ are the f-stop numbers for the imaging lens and the objective lens, respectively; M is the magnification; and CoC is the circle of confusion. The CoC, specified by the experimenter, is the maximum acceptable defocus in the imaging plane. For example, stacking two 50 mm, f1.2 lenses and choosing 10 μm as the CoC results in a $DoF \approx 48\mu m$. In most optical imaging applications, the tissue of interest is several hundred micrometers below the pia mater comprising the cortical surface. For example, thalamocortical projections, carrying specific sensory information, terminate at layer IV of the cortex. Here, synaptic density and metabolic rate is highest and the orientation of the capillary network is isotropic (7) (see Fig. 4 in Ref. 18.). Therefore, the focal plane of the tandem lens is typically positioned accordingly, which is achieved by first manually focusing the system on the cortical surface where numerous anatomical details exist. The camera-and-lens system is then lowered to the desired position by way of a micromanipulator. A minimized DoF, when the focal plane is positioned at depth, defocuses the more superficial blood vessels, which is a desirable outcome given that the hemodynamics of these vessels are

less correlated with synaptic activity and often contribute to artifacts in the acquired data.

3.4. Imaging Device

Optical imaging studies predating the advent of digital cameras employed photodiode arrays. The spatial resolution of such arrays is typically limited, yet photodiodes still find use in conjunction with voltage-sensitive dyes, where fine temporal resolution of transmembrane activity is required (e.g., Grinvald et al. (19) reported the use of a 100-photodiode array over a cortical area of 6 mm × 6 mm), although typically not in applications concerning the intrinsic signal. More details of photodiode use in functional optical imaging can be found in Ebner and Chen (20). Inyushin et al. (14) reported the successful use of a commercially available 8-bit camera to acquire the intrinsic signal from rat barrel cortex, a significant experimental achievement. More typically, a "scientific-grade" camera is required, wherein each photosensitive element is digitized to at least 12 bits (therefore, in the absence of noise, a signal on the order of one part in 4095 may be measured). Scientific-grade cameras are designed with a mind to tightly packing photosensitive elements (the camera used by the present authors comprises elements approximately 7 μm in width) and minimizing noise typical of solid-state imaging devices: thermal noise or dark current, read-out noise, etc. A liquid-cooled scientific-grade camera may demonstrate reduced dark current, increasing the well depth of a sensor, thereby allowing for increased exposure time, and effectively mitigating read-out noise and quantum fluctuations of the signal in low light conditions. The intrinsic signals measured in the anesthetized cat are lowpass filtered with a bandwidth of approximately 0.3 Hz (present authors, unpublished data), suggesting that a frame rate of 0.6 frames per second is sufficient for measurement of the intrinsic signal.

3.5. Image Processing

Processing of the imaging data typically begins with ensemble averaging. A single record, comprised of a temporal sequence of images may be represented by

$$g[\mathrm{k}, n],$$

where k denotes a particular pixel and n a particular frame number ($n = n_0$ denotes stimulus onset). The ensemble average resulting from a number of such records, pertaining to a particular stimulus condition, is therefore

$$\bar{g}_i[\mathrm{k}, n] = \frac{1}{J}\sum_{j=0}^{J-1} g_i^j[\mathrm{k}, n],$$

where the subscript i denotes the stimulus condition and J is the number of records averaged. Assuming that the noise is additive and uncorrelated from record to record (e.g., small fluctuations in the intensity of the light source), then by the central limit theorem, the effect of ensemble averaging is to reduce the power of the noise by a factor of $J^{-1/2}$.

The response to the stimulus, observed in the cortex, is given by the change relative to a prestimulus reference frame r ($r < n_0$)

$$\bar{f}_i[\mathrm{k}, n] = \bar{g}_i[\mathrm{k}, n] - \bar{g}_i[\mathrm{k}, r].$$

This equation is the *first frame method* described by Grinvald et al. (12) and the result is often referred to as the *global signal*, because it effectively depicts those regions of the cortex that respond preferentially to the given stimulus condition as opposed to all other stimulus conditions. Single-condition maps are particularly useful in isolating the signal of interest when imaging highly vascular areas where the global signal may be dominated by changes in blood volume in the vessels. The single-condition map for stimulus condition i is given by

$$f_i[\mathrm{k}] = \bar{f}_i[\mathrm{k}, m] \Big/ f_{CB}[\mathrm{k}],$$

where m denotes the frame number corresponding to the maximal response ($m > n_0$) and $f_{CB}[\mathrm{k}]$ denotes the so-called *cocktail blank*. The cocktail blank is a reference image given by the sum of the maximal response observed in the global signal for each stimulus condition, for example,

$$f_{CB}[\mathrm{k}] = \frac{1}{I}\sum_{i=0}^{I-1} \bar{f}_i[\mathrm{k}, m],$$

where I is the number of stimulus conditions (e.g., eight orientations of a visual stimulus, each orientation rotated by 22.5°) and m is the frame number corresponding to the maximal response (e.g., just subsequent to the cessation of a 2 s visual stimulus). An alternative to the *division* method is the *difference* method, whereby the single-condition map is obtained by subtracting the cocktail blank from the frame corresponding to the maximal response, for example,

$$f_i[\mathrm{k}] = \bar{f}_i[\mathrm{k}, m] - f_{CB}[\mathrm{k}].$$

The experience of the present authors is that the *division* and *difference* equations yield comparable results [see also Bonhoeffer and Grinvald (2)]. However, some care must be taken when the amplitude of the maximal response differs from one stimulus condition to the next. The *difference* method better facilitates statistical analysis, as compared with the *division* method, as the variance is more easily calculated. In the literature, Student's t-test and analysis of variance (ANOVA) are basic models often employed to identify significant changes in the cortical response.

The analysis outlined above describes only the basic operations typically employed and a number of variations on the method exist. For example, the prestimulus reference image, r, may be used as a divisor in an attempt to adjust for uneven illumination, although it may amplify noise in dark regions of the image. Image registration (see entry in this volume) may be performed prior to ensemble

averaging as a means of mitigating movement artifact, and linear filtering (both temporal and spatial) may be used to accentuate the signal amongst movement artifact and speckle noise. Further, Stetter et al. (21) demonstrated in cat and ferret cortex that principal component analysis is an effective means of isolating cortical response from cardiac- and respiration-related artifact, without the requirement for orthogonal stimulus conditions.

4. DISCUSSION AND OUTLOOK

The remainder of this article is devoted to outlining some of the more striking applications of OIIS. Bonhoeffer and Grinvald (22) demonstrated "pinwheels" in the cat visual cortex (specifically, see their Fig. 2). These pinwheels, arrayed semi-regularly across the primary visual cortex, comprise multiple overlapping domains, each of which responds to visual stimulation by way of a drifting luminance grating at a particular orientation. Pinwheel centers, where the multiple domains osculate, are apparently distributed evenly among left-eye and right-eye ocular dominance columns (the domains that respond preferentially to stimulus delivered to one eye or the other) and the pinwheels themselves swirl in outgoing spirals, some clockwise and some counterclockwise. One critical observation to be made here is that within a small area of tissue, all orientations are represented. Therefore, focal stimulation of the retina, which projects to a small, finite area of cortex (19), is accurately represented with regard to its orientation. This "uniformity of coverage" was also reported in Bosking et al. (23), which demonstrated, in the visual cortex of the tree shrew, the fine-scale organization of the retinotopic map. Those authors also reported striking similarity between imaging data and microelectrode measurements of neural spiking when both techniques were applied within the same animal. Bosking et al. identified overlapping domains of neurons each responding to a stimulus occupying only a restricted patch of the visual field, and were able to demonstrate a 100 μm migration of the activated domain in response to a 0.5 degree shift in visual stimulus. Accordingly, those authors have asserted that, for such mapping studies, OIIS provides finer detail as to map organization as compared with electrophysiological techniques; OIIS effectively averages million-fold neuronal responses, whereas microelectrode recordings are perforce confounded by the vagaries of (expansive) dendritic arbors embedded in the electrotonic medium. The Bosking study, in effect, highlights simultaneously an advantage and a shortcoming of OIIS: Although it may provide improved spatial detail regarding the organization of cortical domains, it is effectively blind to the neural code for populations, at which point the experimenter must resort to electrophysiological techniques. It is interesting to note that these pinwheel results corroborate the model of Braitenberg and Braitenberg (24) who, by way of painstaking extrapolation and interpolation of available single-cell data, proposed a concentric organization in cat primary visual cortex [for a subsequent, more developed model, see Swindale (25)].

Optical imaging has revealed overlap of domains as an organizing principle in much mammalian cortex, although not all. Masino et al. ((26), especially their Fig. 4) provide a striking demonstration of nonoverlapping parcellation in rat barrel cortex, that is, the part of the somatosensory cortex devoted to representing mechanical stimulation of the facial whiskers (27). Deflection of a single whisker was shown to elicit optical signals in a domain approximately 900 μm in diameter; data from all whiskers, taken together, was shown to effectively tile the barrel cortex. Interestingly, Masino et al. imaged the cortex through the intact, thinned skull—a significant experimental achievement, obviating the need for a cranial window and significantly reducing artifacts because of pulsation. Harel et al. (28) studied the chinchilla cortex and, within each animal, simultaneously mapped the tonotopy of primary (AI) and secondary (AII) auditory cortices. Although these fields did not overlap, the domains comprising each, that is, clumps of neurons responding preferentially to tones at a particular frequency, overlapped significantly. In the chinchilla, AI and AII are apparently organized along two almost orthogonal axes, each approximately 2 mm in length, forming an "L" shape in the temporal cortex. With increasing frequency of stimulation, cortical representation diverges along these axes. Similar organizing principles have been demonstrated in the cat auditory cortex, in response to both acoustic stimuli and functional electrical stimulation (FES) by way of a cochlear implant (29,30). Here, AI was plastic; 3-month-long electrical stimulation increased the sizes of functional domains and increased the overlap between these domains, corresponding to the decreased selectivity of electrical stimulation as compared with its normal, biological counterpart. By contrast, neonatally deafened controls exhibited a sort of disintegrated organization. Further to FES work done by Dinse et al., Walter et al. (31) demonstrated the retinotopic response of the anesthetized cat visual cortex to electrical stimulation of the intact retina. This study involved a fully implanted prototype neuroprosthesis and associated electrode array (with electrodes separated by approximately 750 μm). Intrinsic signals imaged in the primary visual cortex suggested discrete points, separated by approximately 5.3°, were elicited in the visual field.

Rubin and Katz (32) imaged the rat olfactory bulb. Here, similar receptors on the sensory epithelium converge in the bulb on so-called olfactory glomeruli — dense masses of neuropil, approximately 150 μm in diameter, some 2000 of which comprise the bulb in the rat. These olfactory domains are some of the smallest physiological features optically imaged to date. Rubin and Katz demonstrated that odorants (such as banana oil and peanut butter) similar in chemical structure elicit similar, but nonetheless different, patterns of glomeruli activity in the bulb, which was likewise observed when odorant concentration was varied. Interestingly, similar odors (similar by the standards of human perception), namely "caraway" and "spearmint," elicited near-identical response on the rat bulb. Further experimentation may reveal whether similar odor representations and odor perceptions correlate.

Clearly OIIS has proven to be a powerful technique in exploring the functional organization of cortical activity elicited in response to sensory stimulation, which has been possible because sensory processing remains largely intact under anesthesia. In contrast, higher cognitive functions are significantly depressed under anesthesia, seemingly precluding the utility of OIIS in studying neural activity underlying cognitive processes in the cortex. This apparent shortcoming has motivated a number of groups to investigate the potential for performing OIIS in unanesthetized animals. Among the earliest such studies is that of Grinvald et al. (33), who demonstrated the potential for OIIS in studying cortical activity in awake monkeys, successfully observing functional organisation of the visual cortex consistent with that previously observed under anesthesia. Interestingly, Grinvald et al. reported that the amplitude of the intrinsic signal observed at 630 nm was as much as two to three times larger in awake compared with anesthetized animals.

Based on their success with awake primates, Grinvald et al. (33) proposed the use of OIIS as a clinical tool for assessing normal brain activity in human patients during neurosurgical procedures. Such an application was subsequently reported by Haglund et al. (34), who demonstrated the intraoperative use of OIIS of human cortex exposed *a priori* as part of routine surgical treatment of cortical pathology (e.g., intractable epilepsy or tumor). In one (awake) patient, Haglund et al. showed that the effect of electrical cortical stimulation (which is routine in identifying functional areas bordering diseased tissue due for dissection or excision) on language was correlated with OIIS obtained during a cognitive task, wherein the patient was required to name presented objects. The cortical area concerned was Wernicke's area, an area related to the aforementioned Broca's area, and responsible for language comprehension and speech. In another patient, Haglund et al. imaged the spatial extent and time course of epileptiform afterdischarge (persistent neural activity associated with epileptic seizure) in an area slightly anterior to the motor cortex. Interestingly, some areas of epileptiform activity were bordered by an optical signal that developed opposite polarity. Similar "center-surround" intrinsic signals have also been reported by Tommerdahl et al. (3), who imaged activity in squirrel monkey somatosensory cortex in response to tactile stimulation of the fingers and hand. It has been proposed that the surround activity involves neural inhibition acting between functional domains (in Tommerdahl's case, between domains corresponding to individual fingers or locations on the palm), or the shunting of blood to areas of more synaptic activity, and that this has perceptual correlates, namely, improved spatial discrimination (3,34).

The work of Haglund et al. (34) lends some support to the more widespread intra-operative use of OIIS, in conjunction with electrical cortical stimulation, for the purpose of decision support. However, to date, OIIS has had little clinical impact [see Pouratian et al. (35)], which is largely because of the overwhelming artifact that brain pulsation introduces to data; in clinical settings, as opposed to research settings, a cranial window cannot be used to mitigate pulsation and time constraints limit the amount of data that may be acquired and hence the amount of noise-mitigating averaging that may be performed.

Exposure and illumination of the cortex from above necessarily limits the usefulness of OIIS, in its conventional form, to investigation of neural activity in the uppermost layers of the cortex. The viability of the reflectance signal recorded is determined by the light absorption and scattering characteristics of brain tissue at the wavelengths of interest. Considerable data regarding the light absorption and scattering characteristics of human white and gray matter at wavelengths between 400 nm and 2500 nm may be found in Eggert and Blazek (36). The experience of the present authors suggests a practical upper limit on the depth of tissue that may be imaged somewhere in the vicinity of 1 mm at a wavelength of 605 nm. The results of Eggert and Blazek suggest that the upper limit is likely to be somewhat less at lower wavelengths.

Although the majority of previous optical imaging studies are concerned only with superficial cortical activity, a number of studies have employed OIIS techniques to record neural activity within deep-brain structures. For example, Rector and Harper (37) describe a novel fiber-optic probe and miniaturized CCD camera for chronic imaging of intrinsic signals in the hippocampus of freely behaving cats. Techniques such as this hold great potential for future developmental and behavioral studies.

BIBLIOGRAPHY

1. M. Jueptner and C. Weiller, Review: does measurement of regional cerebral blood flow reflect synaptic activity?—Implications for PET and fMRI, *NeuroImage* 1995; **2**:148–156.
2. T. Bonhoeffer and A. Grinvald, Optical imaging based on intrinsic signals: the methodology. In: A. Toga, and J. C. Mazziotta, eds., San Diego, C A: *Brain Mapping: The Methods*, Academic Press 1996, pp. 55–97.
3. M. Tommerdahl, O. Favorov, and B. L. Whitsel, Optical imaging of intrinsic signals in somatosensory cortex. *Behav. Brain Res.* 2002; **135**:83–91.
4. W. G. Zijlstra and A. Buursma, Spectrophotometry of hemoglobin: absorption spectra of bovine oxyhemoglobin, deoxyhemoglobin, carboxyhemoglobin, and methemoglobin. *Compar. Biochem. Physiol. B-Biochem. Molec. Biol.* 1997; **118**(4):743–749.
5. P. Li, Q. Luo, W. Luo, S. Chen, H. Cheng, and Zeng, Shaoqun, Spatiotemporal characteristics of cerebral blood volume changes in rat somatosensory cortex evoked by sciatic nerve stimulation and obtained by optical imaging. *J. Biomed. Opt.* 2003; **8**(4):629–635.
6. I. Vanzetta, R. Hildesheim, and A. Grinvald, Compartment-resolved imaging of activity dependent dynamics of cortical blood volume and oximetry. *J. Neurosci.* 2005; **25**(9):2233–2244.
7. A. Hudetz, Blood flow in the cerebral capillary network: a review emphasizing observations with intravital microscopy. *Microcirculation (London)* 1997; **4**(2):233–252.
8. E. Shtoyerman, A. Arieli, H. Slovin, I. Vanzetta, and A. Grinvald, Long-term optical imaging and spectroscopy reveal mechanisms underlying the intrinsic signal and stability of

cortical maps in V1 of behaving monkeys. *J. Neurosci*. 2000; **20**(21):8111–8121.

9. J. Mayhew, L. Zhao, Y. Hou, J. Berwick, S. Askew, Y. Zheng, and P. Coffey, Spectroscopic investigation of reflectance changes in the barrel cortex following whisker stimulation In: Hudetz and Bruley, eds., *Oxygen Transport to Tissue*. New York: Plenum Press, 1998, pp. 139–148.
10. R. D. Frostig, E. E. Lieke, D. Y. Ts'o, and A. Grinvald, Cortical functional architecture and local coupling between neuronal activity and the microcirculation revealed by *in vivo* high-resolution optical imaging of intrinsic signals. *Proc. Natl. Acad. Sci. USA* 1990; **87**:6082–6086.
11. D. Malonek and A. Grinvald, Interations between electrical activity and cortical microcirculation revealed by imaging spectroscopy: implications for functional brain mapping. *Science* 1996; **272**(5261):551–554.
12. A. Grinvald, D. Shoham, A. Shmuel, D. E. Glaser, I. Vanzetta, E. Shtoyerman, H. Slovin, A. Sterkin, C. Wijnbergen, R. Hildesheim, and A. Arieli, In-vivo optical imaging of cortical architecture and dynamics. In: U. Windhorst and H. Johansson, eds., *Modern Techniques in Neuroscience Research* Heidelberg: Springer-Verlag, 1999; pp. 893–969.
13. V. A. Kalatsky and M. P. Stryker, New paradigm for optical imaging: temporally encoded maps of intrinsic signal. *Neuron* 2003; **38**(4):529–545.
14. M. Yu. Inyushin, A. B. Vol'nova, and D. N. Lenkov, Use of a simplified method of optical recording to identify foci of maximal neuron activity in the somatosensory cortex of white rats. *Neurosci. Behav. Physiol.* 2001; **31**(2):201–205.
15. H. A. Kontos, Cerebral preparations: advantages and disadvantages. In: C. H. Baker and W.L. Nastuk, eds., *Microcirculatory Technology.* New York: Academic Press, 1986, pp. 55–64.
16. E. H. Ratzlaff and A. Grinvald, A tandem-lens epifluorescence macroscope - hundred-fold brightness advantage for wide-field imaging. *J. Neurosci. Meth.* 1991; **36**(2–3):127–137.
17. S.F. Ray, *Applied Photographic Optics.* Boston, MA: Focal Press, 1988.
18. C.Kennedy, M. H. Des Rosiers, O. Sakurada, M. Shinohara, M. Reivich, J. W. Jehle, and L. Sokoloff, Metabolic mapping of the primary visual system of the monkey by means of the autoradiographic ^{14}C-deoxyglucose technique. *Proc. Natl. Acad. Sci. USA* 1976 **73**(11):4230–4234.
19. A. Grinvald, E. E. Lieke, R. D. Frostig, and R. Hildesheim, Cortical point-spread function and long-range lateral interactions revealed by real-time optical imaging of macaque monkey primary visual cortex. *J. Neurosci.* 1994; **14**(5):2545–2568.
20. T. J. Ebner and G. Chen, Use of voltage-sensitive dyes and optical recordings in the central nervous system. *Progr. Neurobiol.* 1995; **46**(5):463–506.
21. M. Stetter, I. Schiessl, T. Otto, F. Sengpiel, M. Hubener, T. Bonhoeffer, and K. Obermayer, Principal component analysis and blind separation of sources for optical imaging of intrinsic signals. *Neuroimage* 2000; **11**(5):482–490.
22. T. Bonhoeffer and A. Grinvald, Iso-orientation domains in cat visual cortex are arranged in pinwheel-like patterns**.** *Nature* 1991; **353**(6343):429–431.
23. W. H. Bosking, J. C. Crowley, and D. Fitzpatrick, Spatial coding of position and orientation in primary visual cortex. *Nature Neurosci.* 2002; **5**:874–882.
24. V. Braitenberg and C. Braitenberg, Geometry of orientation columns in the visual-cortex. *Biolog. Cybernet.* 1979; **33**(3):79–186.
25. N. V. Swindale, A model for the formation of orientation columns. *Proc. Royal Soc. London Series B* 1982; **215**: 211–230.
26. S. A. Masino, M. C. Kwon, Y. Dory, and R. D. Frostig, Characterization of functional organization within rat barrel cortex using intrinsic signal optical imaging through a thinned skull. *Proc. Natl. Acad. Sci. USA* 1993; **90**:9998–10002.
27. T. A. Woolsey and H. van der Loos, Structural organisation of layer IV in somatosensory region (SI) of mouse cerebral cortex. Description of a cortical field composed of discrete cytoarchitectonic units. *Brain Res.* 1970; **17**(2):205–242.
28. N. Harel, N. Mori, S. Sawada, R. J. Mount, and R. V. Harrison, Three distinct auditory areas of cortex (AI, AII, and AAF) defined by optical imaging of intrinsic signals. *NeuroImage* 2000; **11**:302–312.
29. H.R. Dinse, B. Godde, T. Hilger, G. Reuter, S.M. Cords, T. Lenarz, and W. von Seelen, Optical imaging of cat auditory cortex cochleotopic selectivity evoked by acute electrical stimulation of a multi-channel cochlear implant. *Eur. J. Neurosci.* 1997; **9**:113–119.
30. H.R. Dinse, B. Godde, G. Reuter, S.M. Cords, and T. Hilger, Auditory cortical plasticity under operation: reorganization of auditory cortex induced by electric cochlear stimulation reveals adaptation to altered sensory input statistics. *Speech Commun.* 2003; **41**:201–219.
31. P. Walter, Z. F. Kisvarday, M. Gortz, N. Alteheld, G. Rossler, T. Stieglitz, and U. T.Eysel, Cortical activation via an implanted wireless retinal prosthesis. *Invest. Ophthalmol. Vis. Sci.* 2005; **46**(5):1780–1785.
32. B. D. Rubin and L. C. Katz, Optical imaging of odorant representations in the mammalian olfactory bulb. *Neuron* 1999; **23**:499–511.
33. A. Grinvald, R. D. Frostig, R. M. Siegel, and E. Bartfeld, High-resolution optical imaging of functional brain architecture in the awake monkey. *Proc. Natl. Acad. Sci. USA* 1991; **88**:11559–11563.
34. M. M. Haglund, G. A. Ojemann, and D. W. Hochman, Optical imaging of epileptiform and functional activity in human cerebral cortex. *Nature* 1992; **358**:668–671.
35. N. Pouratian, S.A. Sheth, N.A. Martin, and A.W. Toga, Shedding light on brain mapping: advances in human optical imaging. *Trends Neurosci.* 2003; **26**(5):277–282.
36. H. R. Eggert and V. Blazek, Optical properties of normal human intracranial tissue in the spectral range of 400 nm to 2500 nm. *Optical Imaging of Brain Function and Metabolism in Advances in Experimental Medicine and Biology.* U. Dirnagl, A. Villringer, and K. M. Einh, eds., New York: Plenum Press, 1993, pp. 47–55.
37. D. M. Rector and R. M. Harper, Imaging of hippocampal neural activity in freely behaving animals. *J. Behav. Brain Res.* 1991; **42**(2):143–149.